Nuclear charge radii of molybdenum fission fragments

F.C. Charlwood [a,*], K. Baczynska [b], J. Billowes [a], P. Campbell [a], B. Cheal [a], T. Eronen [c], D.H. Forest [b], A. Jokinen [c], T. Kessler [c], I.D. Moore [c], H. Penttilä [c], R. Powis [b], M. Rüffer [b], A. Saastamoinen [c], G. Tungate [b], J. Äystö [c]

[a] *Schuster Building, The University of Manchester, Manchester M13 9PL, UK*
[b] *School of Physics and Astronomy, The University of Birmingham, Edgbaston, Birmingham B15 2TT, UK*
[c] *Department of Physics, University of Jyväskylä, PB 35 (YFL) FIN-40351 Jyväskylä, Finland*

A R T I C L E   I N F O

A B S T R A C T

Radioisotopes of molybdenum have been studied using laser spectroscopy techniques at the IGISOL facility, University of Jyväskylä. Differences in nuclear charge radii have been determined for neutron deficient isotopes ^{90,91}Mo and neutron rich isotopes $^{102-106,108}$Mo (and all stable isotopes). A smooth transition in the mean square charge radii is observed as the neutron number increases with no sudden shape change observed in the region around $N = 60$. As N increases, the nuclear deformation appears to go beyond a maximum and a fall off at $N = 66$ is observed. The magnetic moments of the odd isotopes ^{91,103,105}Mo are also determined.

© 2009 Elsevier B.V. All rights reserved.

High resolution optical measurements provide sensitive, model independent nuclear structure data [1,2]. Through the analysis of hyperfine structures and isotope shifts nuclear parameters can be extracted. In particular, laser spectroscopy provides the only known method for determining the charge radii of radioactive nuclei and is sensitive enough to allow long chains of isotopes to be studied to the limits of stability and fast enough to permit the study of short-lived species.

The element molybdenum ($Z = 42$) cannot be efficiently produced by conventional ion source techniques due to its low vapour pressure. At the IGISOL [3] facility at the University of Jyväskylä (JYFL), Finland, all elements can be produced with fast extraction times, including those of a refractory nature such as Mo.

In this work, the first radioactive isotope shift and charge radii measurements, performed on the singly-charged Mo ion, are presented. The molybdenum ionic ground state shows the special characteristics displayed by all half-filled electronic shell structures (d^5 in this case). The $^6S_{5/2}$ lowest state is extremely well bound and recouplings of this configuration form a high density of excited metastable states at an excitation of $\sim$1.5 eV. As a result, deep UV wavelengths are required for spectroscopy from the ionic Mo ground state. If atomic spectroscopy is attempted, charge exchange with alkali vapours populates the atom in the high level density of core-excited metastable states with only small populations in individual states.

With respect to the nuclear structure, nuclei in the $Z \sim 40$, $N \sim 60$ region exhibit a substantial sub-shell gap in a region of otherwise high level density. On addition of neutrons from the magic shell gap at $N = 50$, nuclei undergo transitions from spherical to prolate (and oblate) deformations as $N = 60$ is approached and crossed. A *sudden* onset of deformation has been well established for isotopic chains centred on $Z = 39$ (though the form of this transition is a long standing dispute [4]). Evidence for an abrupt shape change include, for example, 2^+ lifetime measurements [5] in Sr and Zr, where the B(E2) values are relatively constant before rapidly increasing at $N = 60$. Measurements of magnetic moments, which near perfectly agree with spherical Schmidt estimates for $N < 60$ [6] and the existence of 0^+ first excited states in ^{96,98}Zr also appear to support a transition being one that is from near-spherical to strongly deformed. Fission fragment spectroscopy with the EUROGAM2 array [7] has however suggested that a smoother transition in shape change occurs with the work observing no rotational bands nor large quadrupole moments in excited states for $N < 60$. Rovibrational states however were found at higher excitation energy in nuclei for $N > 60$. Optical measurements [4,6,8,9] of the charge radii differences in this region closely reflect these results but suggest a significant departure from sphericity before the sudden shape change. Studies of the yttrium isomers [4] show

---

prior to $N = 60$ relatively small quadrupole moments and suggest a dynamic nature in this deformation. Measurements on ruthenium ($Z = 44$) charge radii [10] using classical spectroscopy, show no sharp change at $N = 60$.

Data were obtained with the IGISOL [3] (Ion guide separator on-line) using a variety of off-line and on-line production methods. On-line reactions included proton induced fission at 33 MeV on a natural uranium target $^{nat}U(p,f)^{92-108}Mo$, fusion evaporation reactions $^{93}Nb(p,3n)^{91}Mo$ and $^{92}Mo(p,pxn)^{90,91}Mo$. Typical ion fluxes were $3000\ s^{-1}$ for ^{91}Mo and $250\ s^{-1}$ for ^{108}Mo. Recoiling ions in the ion guide were efficiently thermalised and extracted using a helium buffer gas and a sextupole ion guide (SPIG). Mass-analysed ensembles were then cooled and bunched in an RF quadrupole trap [11] and accelerated to a laser-ion interaction region. A tuning voltage was applied to this region to Doppler tune ionic ensembles onto resonance. Resolved hyperfine resonances were then observed as a function of accelerating voltage. An intense reference peak in a chosen isotope was measured between all experimental scans such that the data could be later corrected for any voltage and frequency drifts.

Non-resonant laser scattering of photons account for the majority of the experimental background ($\sim200\ s^{-1}$). Background reduction methods involved accumulating the ions for 100–200 ms and then releasing in 15 μs bunches. The data acquisition system was gated to only accept photons during the time window (~15 μs) of the ion bunch traversing the light collection region.

A continuous wave, frequency-doubled dye laser was used for production of UV light at a fixed wavelength of 293.43 nm. The maximum power used was 0.7 mW. This stabilised laser light was focussed and overlapped with the ion beam at the light collection region in a collinear geometry. The laser wavelength corresponds to that of a transition in Mo^+ from the first excited state, $4d^45s\ ^6D_{1/2}$, at $11783.36\ cm^{-1}$, to a state, $4d^45p\ ^6F_{1/2}$, at $45853.08\ cm^{-1}$.

Bunched beam spectroscopy would typically, by necessity, utilise a transition from the ionic ground state (into which all populations relax during bunching). In Mo^+ such a ground state transition would have a wavelength in the deep UV (~210 nm), and thus spectroscopy at JYFL was initially approached using an optical pumping technique recently developed at the facility [12]. However, unlike all other elements studied at the laser-IGISOL, a naturally enhanced population of the 1st excited state was observed independent of production mechanism. This population was further observed to survive many hundreds of milliseconds' storage in the cooler-buncher. The uniform, production-independent, state populations may well be due to redistribution of states on the ions passage through the SPIG [13]. At JYFL, metastable states are observed to be populated in this device and ensembles which have been optically pumped prior to injection are observed to be redistributed upon extraction. Typically (for all cases bar Mo) such populations are subsequently relaxed in the RFQ cooler-buncher. Excitations in Mo^+ however populate a substantial fraction of states built on a d^4s configuration, very differently structured to the d^5 configuration of the ground state. Once these populations relax into the lowest metastable state, the $4d^45s\ ^6D_{1/2}$, a bottleneck is apparently reached with further relaxation to the ground state severely hindered.

Spectroscopic efficiencies, of ~1 photon per 3000 ions, comparable or better than that of ground state transitions studied in other ions were achieved and exploited. A full investigation of this (to date unique) metastable population is underway at JYFL where the optical pumping of the d^5 ground state is under study. With respect to the measurement of nuclear parameters it has already been spectroscopically possible to study all ions produced at greater than 100 ions per second using this large, long-lived natural metastable fraction. A further ionic transition, $4d^45s\ ^6D_{1/2}$

$(11783.36\ cm^{-1}) \rightarrow 4d^45p\ ^6F_{3/2}$ ($46148.12\ cm^{-1}$), was explored for the stable Mo isotopes and used to uniquely assign the hyperfine parameters in the 293.43 nm transition.

Spectroscopically, if the frequency of a transition occurs at v^A for isotope A and $v^{A'}$ for isotope A' the isotope shift can be conventionally expressed as:

$$\delta v_{IS}^{A,A'} = v^{A'} - v^A. \tag{1}$$

Hyperfine structure arises from the interaction of the nuclear charge distribution and the electromagnetic field generated by the orbital electrons and further perturbs the atomic states of a transition. Combining the magnetic dipole and electric quadrupole components gives the first order hyperfine interaction as

$$E_{F,J}^{(1)} = \frac{AK}{2} + \frac{B}{4} \frac{\frac{3}{2}K(K+1) - 2I(I+1)J(J+1)}{I(2I-1)J(2J-1)}, \tag{2}$$

where $K = F(F+1) - I(I+1) - J(J+1)$. The resultant angular momentum, F is the vector sum of the nuclear, I, and electronic, J, spins. These perturbations are given relative to the energy of the unperturbed state. The magnetic hyperfine structure constant, A, and electric quadrupole hyperfine structure constant, B, are related to the nuclear magnetic moment, μ and quadrupole moment, Q_s, by [1],

$$A = \frac{\mu B_e}{IJ}, \tag{3a}$$

$$B = eQ_s \left\langle \frac{\partial^2 V_e}{\partial z^2} \right\rangle. \tag{3b}$$

Figs. 1 and 2 show resonances observed from the stable and radioactive isotopes respectively. A first order hyperfine fit to all observed resonance peaks in the experimental spectra was made using Voigt profiles (convolutions of Gaussian and Lorentzian lineshapes) by minimising the χ^2. A typical, power broadened linewidth of ~65 MHz was observed and the reduced χ^2 ranged from $0.9 \rightarrow 1.6$ for all spectra. Hyperfine A parameters and isotope shift values were evaluated from this full structure fit and are displayed in Table 1. No quadrupole moment data could be obtained for the radioactive isotopes due to the requirement that $J \geqslant 1$ for an electric field gradient ($\partial^2 V_e / \partial z^2$) to be produced at the nucleus. A possible systematic error from the reading of acceleration voltage, 0.1%, introduces a systematic scaling uncertainty of $\sim1\%$ in the values of the isotope shifts.

A second transition was studied to ascertain the sign of the hyperfine A coefficients (as two solutions otherwise exist for the studied line). A spectrum for the stable isotope ^{95}Mo is shown in Fig. 1 for the transition $4d^45s\ ^6D_{1/2} \rightarrow 4d^45p\ ^6F_{3/2}$. Hyperfine A parameters of ^{95}Mo were determined to be negative (with the upper $4d^45p\ ^6F_{3/2}$ state $A = -135.9(3)$ MHz and $B = 0(2)$ MHz).

An atomic anomaly [14] of 0.17% was detected in the ratio of A coefficients, between ^{95}Mo and ^{97}Mo, for the states of the 293.43 nm transition. This small contribution to the uncertainty on extracted magnetic moments has been neglected here. The accurately known magnetic moments [15] of ^{95}Mo and ^{97}Mo, $\mu = -0.9142(1)\mu_N$ and $\mu = -0.9335(1)\mu_N$ respectively, were used to provide an average calibration of the atomic magnetic field produced by the atomic electrons, B_e. Table 2 shows the magnetic moments determined in this work.

Fluorescence spectra of ^{103}Mo and ^{105}Mo were fitted with weak field angular coupling estimates of peak intensities for the spin range $I = 3/2 - 9/2$. A clear and significant minimum for $I = 3/2$ was determined in ^{103}Mo that is consistent with the suggested spin assignment [16,17]. The lower statistics in (and higher spin of) ^{105}Mo limited the spin assignment to $I > 3/2$. The suggestion of an $I = 5/2$ in the configuration $[532]5/2^-$ [18,19] is thus compatible with the observed structure.
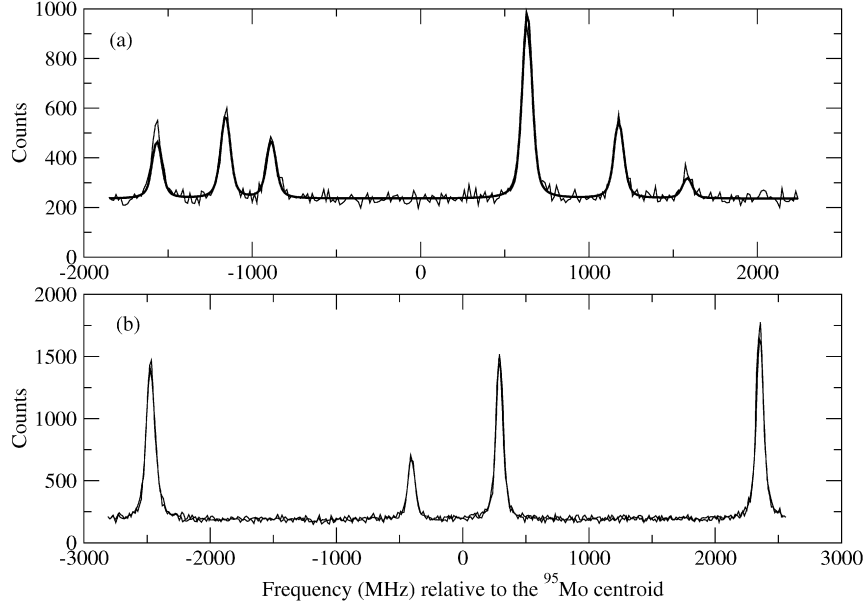
Fig. 1. Hyperfine spectra observed in stable ^{95}Mo. (a) The transition $4d^4 5s\,^6D_{1/2}$ (11783.36 cm^{-1}) $\rightarrow$ $4d^4 5p\,^6F_{3/2}$ (46148.12 cm^{-1}) with a fit included and (b) the transition $4d^4 5s\,^6D_{1/2}$ (11783.36 cm $^{-1}$) $\rightarrow$ $4d^4 5p\,^6F_{1/2}$ (45853.08 cm^{-1}).
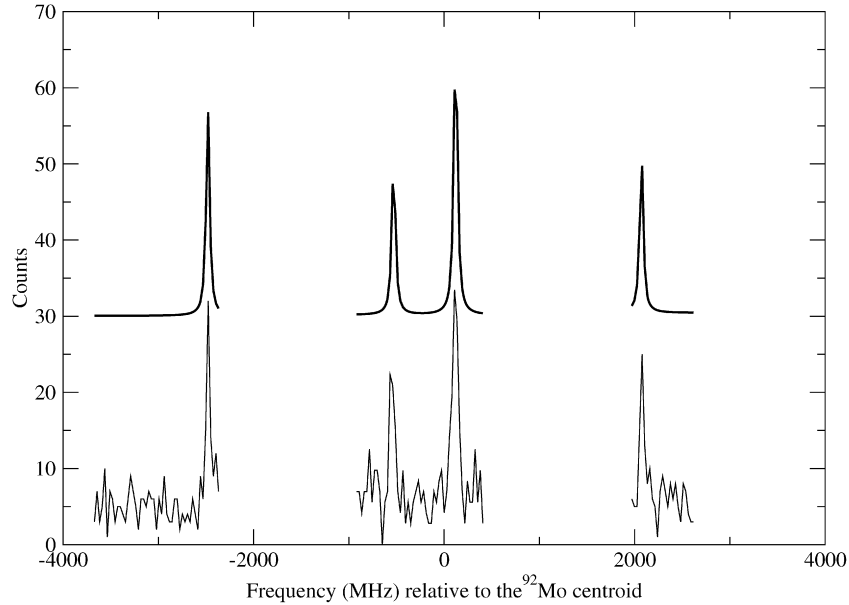

Fig. 2. Fitted resonance spectrum for ^{91}Mo observed on the transition $4d^4 5s\,^6D_{1/2}$ (11783.36 cm^{-1}) $\rightarrow$ $4d^4 5p\,^6F_{1/2}$ (45853.08 cm^{-1}). The fit is displaced from the data, by 25 counts, for clarity.

The change in the mean square charge radius, $\delta\langle r^2 \rangle^{A,A'}$, was determined from the isotope shift (with the above spin assignments) through the relation:

$$\delta \nu^{A,A'} = \left(\frac{A' - A}{AA'} \right) M_i + F_i \delta\langle r^2 \rangle^{A,A'}. \tag{4}$$

The mass and field shift parameters were calibrated using a King plot [20] of the seven stable molybdenum isotopes and model-independent measures of the radial changes. The combined analysis of $\delta\langle r^2 \rangle^{A,A'}$ from Fricke et al. [21] was taken in the analysis. The plot gave an atomic field parameter of $F = -3024(91)$ MHz fm^{-2} and nuclear mass shift $\delta\nu_{MS}^{96,98} = +195(25)$ MHz. These, strongly covariant, parameters were then used to determine $\delta\langle r^2 \rangle^{A,A'}$ for the radioactive isotopes in the chain, shown in Table 2. Systematic scaling errors on $\delta\langle r^2 \rangle$ arising from the

calibration, are dominated by the uncertainties on absolute non-optical measurements of $\langle r^2 \rangle$ [21].

For a quadrupoloid, the mean square charge radii are related to mean square deformation, $\langle \beta_i^2 \rangle$, by

$$\langle r^2 \rangle = \langle r^2 \rangle_{sph} + \langle r^2 \rangle_{sph} \frac{5}{4\pi} \sum_i \langle \beta_i^2 \rangle. \tag{5}$$

The droplet model [22] may be used to provide an estimate of $\langle r^2 \rangle_{sph}$ and the summation assumed to be dominated by the changes in the β_2 quadrupole shape parameter [1]. The radial changes can thus be used to estimate the changes in quadrupole deformation, with β_2^2 incorporating both static and dynamic deformations.

Fig. 3(a) shows that the $\delta\langle r^2 \rangle$ of the molybdenum isotopes follow the general charge radii trends in the $N = 50$ region. However

in contrast to the Sr, Y and Zr chains, no sudden increase is seen in the charge radii at $N = 60$. In the Sr, Y and Zr chains, the nuclei become soft and a small increase in the dynamic quadrupole deformation is seen before a sharp transition. Beyond $N = 60$ the charge radii and non-optical measurements are compatible with a predominantly rigid prolate deformation. Yttrium achieves the highest relative deformation and shows the greatest $N = 50$–60 differences in charge radii. Trends in the Mo isotopes are however markedly different. Changes in the mean square charge radii are significantly lower in Mo and rise steadily from the shell closure. No abrupt changes in $\delta\langle r^2 \rangle$ are observed (except at the $N = 50$ magic shell closure). The measurements of the molybdenum charge radii extend further in neutron number than any other isotope chain in this region. A decrease in the rate of change of charge radius is observed at $N = 66$.

The course of the charge radius closely reflects experimental trends seen in the neutron separation energies. The IGISOL Penning trap group have recently reported new and improved mass mea-surements [23–25] in this region. As shown in Fig. 3(b), two neutron separation energies show a change in character near $N = 60$. The effect is most prominent in yttrium but decreases rapidly with increasing Z. At Mo, the change is almost imperceptible. Molybdenum appears with respect to both charge radii and mass measurements, to be on the border of this region of deformation. Comparing the mass and charge radii measurements, no differential effects are seen with increasing neutron excess. Hager et al. [24] report that beyond $N = 60$, the isotopic chains display an almost linear behaviour with S_{2n} isotonic lines for $Z \geqslant 42$ shown to be nearly parallel [23]. No evidence of further deformation or shell structure changes are observed.

The loss of a well defined shape change and the end of the strongly deformed region at $Z \sim 40$, $N \sim 60$ are predicted to significantly different degrees by the currently available nuclear models. Global calculations of Möller et al. [32] predict in Mo that the quadrupole deformation is greatest at $N = 65$ (compatible with the radii reported here) and then suggest a continuous decrease of

Table 1

Isotope shifts and hyperfine A parameters for the upper ($^6F_{1/2}$) and lower ($^6D_{1/2}$) states experimentally determined using the ionic transition at 293.43 nm. Isotope shift values ($\delta\nu^{A,A'}$) are given relative to $A = 92$. Statistical errors are given in curved brackets and total errors, including scaling systematic uncertainties, in square brackets.

A	I^π	$A(^6F_{1/2})$ (MHz)	$A(^6D_{1/2})$ (MHz)	$\delta\nu^{92,A}$ (MHz)
90	0^+	–	–	−475(3)[9]
91	$9/2^+$	−390.1(7)	−520.3(8)	−171(2)[5]
92	0^+	–	–	0
94	0^+	–	–	−762(1)[9]
95	$5/2^+$	−688.4(5)	−919.7(5)	−925(1)[13]
96	0^+	–	–	−1390(1)[16]
97	$5/2^+$	−702.2(6)	−940.0(6)	−1391(1)[21]
98	0^+	–	–	−1842(1)[20]
100	0^+	–	–	−2645(1)[33]
102	0^+	–	–	−3635(7)[42]
103	$3/2^+$	−335(3)	−447(4)	−4156(7)[46]
104	0^+	–	–	−4353(6)[46]
105	$(5/2^-)$	−417(5)[a]	−552(6)[a]	−4644(8)[53][a]
106	0^+	–	–	−4836(8)[56]
108	0^+	–	–	−4992(8)[63]

[a] Assuming a spin of $I = 5/2$.

Table 2

Magnetic moments and $\delta\langle r^2 \rangle$ values obtained in this work. $\delta\langle r^2 \rangle$ values are given relative to $A = 92$. Statistical and scaling systematic errors are given in curved and square brackets respectively. Column 3 shows the $\delta\langle r^2 \rangle$ values of Fricke et al. [21] used in the calibration.

A	I^π	$\mu(\mu_N)$	$\delta\langle r^2 \rangle^{92,A}$ (fm²)[a]	$\delta\langle r^2 \rangle^{92,A}$ (fm²)
90	0^+	–	–	+0.084(1)
91	$9/2^+$	−0.932(3)	–	+0.021(1)
92	0^+	–	0	0
94	0^+	–	0.321(4)	+0.322[3]
95	$5/2^+$	−0.9142(1)[b]	0.408(4)	+0.410[26]
96	0^+	–	0.600(4)	+0.597[11]
97	$5/2^+$	−0.9335(1)[b]	0.635(6)	+0.630[12]
98	0^+	–	0.820(6)	+0.811[20]
100	0^+	–	1.139(4)	+1.139[39]
102	0^+	–	–	+1.526(1)[70]
103	$3/2^+$	−0.27(2)	–	+1.727(1)[90]
104	0^+	–	–	+1.821(1)[100]
105	$(5/2^-)$	−0.55(2)[c]	–	+1.945(2)[114][c]
106	0^+	–	–	+2.036(2)[125]
108	0^+	–	–	+2.140(2)[138]

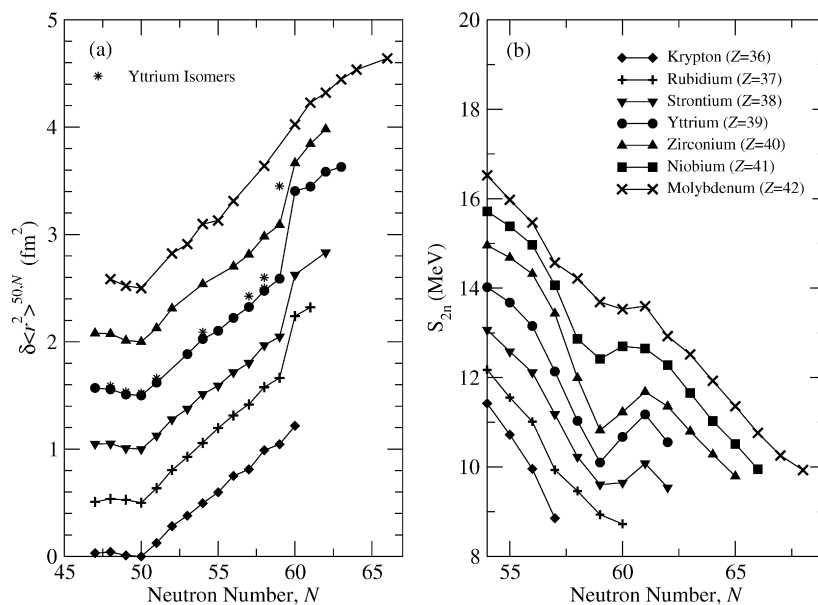[a] Ref. [21].   [b] Ref. [15].   [c] Assuming $I = 5/2$.

Fig. 3. (a) Difference in mean square charge radii in the $N = 60$ region shown for krypton [26], rubidium [8], strontium [9,27], yttrium [4], zirconium [6] and molybdenum given relative to $N = 50$. Each isotone chain is set apart by 0.5 fm² for clarity. (b) Two neutron separation energies shown for krypton, rubidium, strontium, yttrium, zirconium, niobium and molybdenum [23–25,28–30]. Relative errors are smaller than the symbol sizes.
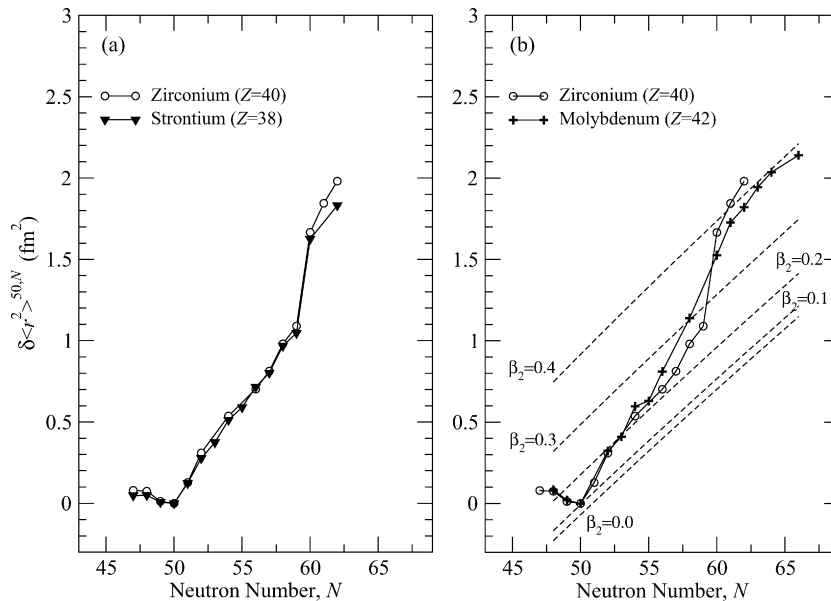
Fig. 4. (a) Comparison of the zirconium [6] and strontium [9,27] mean square charge radii as a function of neutron number. Data are normalized to $N = 50$. (b) Differences between zirconium [6] and molybdenum charge radii over the $N = 50$ shell closure and $N = 60$ shape change. The dashed β_2 isodeformation lines are calculated using the droplet model [22] and normalised to the β_2 value deduced from B(E2) measurements [31] for ^{92}Mo.

deformation until $N = 74$. Earlier calculations [33] had predicted that a significant *oblate* deformation would develop in the ground state at $N = 71$. Potential energy calculations of Skalski et al. [34] suggest an oblate/prolate shape coexistence that, in Mo, is already favouring an oblate ground state at $N = 66$. The absolute magnitude of the oblate deformation is less than that observed in the prolate minimum and (in the absence of sign information) this prediction is also compatible with the measured charge radii. Future measurements utilising a different atomic transition will give access to experimental quadrupole moments across the isotope chain and explore the rate of decrease in mean square charge radius as neutron number increases yet further from stability.

A detailed comparison of the trend of the deformation, beyond the scope of the models above, is made in Fig. 4. Zirconium charge radii undergo a rapid transition at $N = 60$ which is almost identical to that in strontium (Fig. 4(a)). As the proton number is increased to $Z = 42$, a more gradual transition in the region $N = 50$–60 is observed (Fig. 4(b)). Isotonically, it is clear that the deformed $N = 60$, $A = 100$ region is symmetrically centred around Y ($Z = 39$). The Mo measurements reported here mark the "wash out" point of the well defined strongly deformed shapes with respect to the upper limits of both Z and N.

Acknowledgements

References

[1] E.W. Otten, Nuclear radii and moments of unstable isotopes, in: D.A. Bromley (Ed.), Treatise on Heavy-Ion Science, vol. 8, Plenum, New York, 1989, p. 517.
[2] J. Billowes, P. Campbell, J. Phys. G 21 (1995) 707.
[3] J. Äystö, Nucl. Phys. A 693 (2001) 477.
[4] B. Cheal, et al., Phys. Lett. B 645 (2007) 133.
[5] H. Mach, et al., Nucl. Phys. A 523 (1991) 197.
[6] P. Campbell, et al., Phys. Rev. Lett. 89 (2002) 082501.
[7] W. Urban, et al., Nucl. Phys. A 689 (2001) 605.
[8] C. Thibault, et al., Phys. Rev. C 23 (1981) 2720.
[9] F. Buchinger, et al., Phys. Rev. C 41 (6) (1990) 2883.
[10] W.H. King, Proc. R. Soc. A 280 (1964) 430.
[11] A. Nieminen, et al., Phys. Rev. Lett. 88 (9) (2002) 094801.
[12] P. Campbell, Hyp. Interact. 171 (2006) 143.
[13] P. Karvonen, I.D. Moore, et al., Nucl. Instrum. Methods B 266 (2008) 4794.
[14] A. Bohr, V.W. Weisskopf, Phys. Rev. 77 (1950) 94.
[15] W.G. Proctor, F.C. Wu, Phys. Rev. 81 (1) (1951) 20.
[16] K. Shizuma, et al., Z. Phys. A 315 (1984) 65.
[17] K. Liang, et al., Z. Phys. A 346 (1993) 101.
[18] M.A.C. Hotchkis, et al., Nucl. Phys. A 530 (1991) 111.
[19] K. Liang, et al., Z. Phys. A 351 (1995) 13.
[20] W. King, Isotope Shifts in Atomic Spectra, Plenum, New York, 1984.
[21] G. Fricke, K. Heilig, Nuclear Charge Radii, Landolt–Börnstein – Group I Elementary Particles, Nuclei and Atoms, Springer, Berlin, 2004, Chapter 20, p. 1.
[22] D. Berdichevsky, F. Tondeur, Z. Phys. A 322 (1985) 141.
[23] U. Hager, et al., Nucl. Phys. A 793 (2007) 20.
[24] U. Hager, et al., Phys. Rev. Lett. 96 (2006) 042504.
[25] S. Rinta-Antila, et al., Eur. Phys. J. A 31 (2007) 1.
[26] M. Keim, et al., Nucl. Phys. A 586 (1995) 219.
[27] P. Lievens, et al., Phys. Lett. B 256 (1991) 141.
[28] A. Kankainen, et al., Eur. Phys. J. A 29 (2006) 271.
[29] S. Rahaman, et al., Eur. Phys. J. A 32 (2007) 87.
[30] G. Audi, et al., Nucl. Phys. A 729 (2003) 337.
[31] S. Raman, et al., At. Data Nucl. Data Tables 36 (1987) 1.
[32] P. Möller, et al., At. Data Nucl. Data Tables 94 (5) (2008) 758.
[33] P. Möller, et al., At. Data Nucl. Data Tables 59 (2) (1995) 185.
[34] J. Skalski, et al., Nucl. Phys. A 617 (1997) 282.